Journal of Applied Physics

RESEARCH ARTICLE | FEBRUARY 16 2024

Study on the effect of Bi/Sr ratio on the device characteristics of high-T_c superconducting terahertz wave emitters made of $Bi_2Sr_2CaCu_2O_{8+\delta}$ single crystals

M. Nakayama; S. Nakagawa ; T. Yamaguchi; H. Minami; K. Kadowaki ; H. Nakao ; T. Mochiku ; M. Tsujimoto ; S. Ishida ; H. Eisaki ; T. Kashiwagi

Check for updates

J. Appl. Phys. 135, 073902 (2024)
https://doi.org/10.1063/5.0188077

View Online
Export Citation

Articles You May Be Interested In

Improved excitation mode selectivity of high- T c superconducting terahertz emitters

J. Appl. Phys. (July 2018)

Study of device characteristics of intrinsic Josephson junction terahertz emitters related to annealing conditions of the crystals

J. Appl. Phys. (April 2023)

Numerical simulation of quench initiation and propagation in multi-filamentary $Bi_2Sr_2CaCu_2O_x$ round wires at high magnetic fields

J. Appl. Phys. (April 2019)

08 October 2024 06:40:49

Challenge us.
What are your needs for periodic signal detection?
Zurich Instruments
Find out more

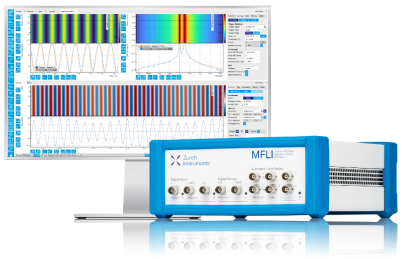

AIP Publishing

Journal of Applied Physics ARTICLE pubs.aip.org/aip/jap

Study on the effect of Bi/Sr ratio on the device characteristics of high-T_c superconducting terahertz wave emitters made of $Bi_2Sr_2CaCu_2O_{8+\delta}$ single crystals

Cite as: J. Appl. Phys. **135**, 073902 (2024); doi: 10.1063/5.0188077
Submitted: 18 November 2023 · Accepted: 24 January 2024 ·
Published Online: 16 February 2024

View Online Export Citation CrossMark

M. Nakayama,[1,2] S. Nakagawa,[1,2] T. Yamaguchi,[1] H. Minami,[1,3] K. Kadowaki,[3] H. Nakao,[4] T. Mochiku,[5] M. Tsujimoto,[6] S. Ishida,[2] H. Eisaki,[2] and T. Kashiwagi[1,3,a)]

AFFILIATIONS

[1]Graduate School of Pure & Applied Sciences, University of Tsukuba, 1-1-1 Tennodai, Tsukuba, Ibaraki 305-8573, Japan
[2]Research Institute for Advanced Electronics and Photonics, National Institute of Advanced Industrial Science and Technology (AIST), 1-1-1 Umezono, Tsukuba, Ibaraki 305-8568, Japan
[3]Division of Materials Science, Faculty of Pure & Applied Sciences, University of Tsukuba, 1-1-1, Tennodai, Tsukuba, Ibaraki 305-8573, Japan
[4]Photon Factory, Institute of Materials Structure Science, High Energy Accelerator Research Organization (KEK), Tsukuba, Ibaraki 305-0801, Japan
[5]National Institute for Materials Science (NIMS), 1-2-1 Sengen, Tsukuba, Ibaraki 305-0047, Japan
[6]Global Research and Development Center for Business by Quantum-AI Technology (G-QuAT), National Institute of Advanced Industrial Science and Technology (AIST), Central 2, 1-1-1 Umezono, Tsukuba, Ibaraki 305-8568, Japan

[a)]**Author to whom correspondence should be addressed:** kashiwagi@ims.tsukuba.ac.jp

08 October 2024 06:40:49

ABSTRACT

To obtain high-performance THz-wave-emitting devices made of single crystals of $Bi_2Sr_2CaCu_2O_{8+\delta}$ (Bi2212), a high-temperature superconductor, an understanding of the device characteristics based on crystal characteristics can be a key issue because, in principle, the electrical properties of the intrinsic Josephson junctions (IJJs) constructed in Bi2212 crystals highly depend on crystal conditions, such as carrier concentration, crystal homogeneities, and crystal defects. To evaluate the tendencies of the device characteristics associated with crystal characteristics, we prepared Bi2212 crystals with different Bi/Sr ratios ($x = 0.05$, 0.15, and 0.25) and δ values (annealed under N_2 or O_2 gas flow conditions). The unit cell parameter c decreased as the Bi/Sr ratio or δ increased. For the same annealing conditions under N_2 gas flow, the superconducting transition temperature as well as the size of the hysteresis loop of the current–voltage characteristics and emission characteristics were significantly suppressed for the sample with $x = 0.25$ compared with the corresponding values for the samples with $x = 0.05$ and 0.15. The experimental results clearly indicate that parameters, such as the Bi/Sr ratio and annealing conditions, are crucial factors in determining the electrical characteristics of a device. This information can be a useful guide for the preparation of crystals for IJJ THz-wave devices that can be fine-tuned according to the desired device characteristics.

© 2024 Author(s). All article content, except where otherwise noted, is licensed under a Creative Commons Attribution-NonCommercial-NoDerivs 4.0 International (CC BY-NC-ND) license (https://creativecommons.org/licenses/by-nc-nd/4.0/). https://doi.org/10.1063/5.0188077

I. INTRODUCTION

Electromagnetic waves in the terahertz frequency range (THz wave) have great potential in fundamental and applied research fields in material sciences because the vibration modes of molecules, polymers, and proteins exist in the frequencies of the THz region. High-performance THz wave emitters, detectors, and related devices have been used in many applications, such as nondestructive inspections, security checking, identification of chemical substances, and cancer detection.[1–4]

© Author(s) 2024

Among THz wave emitters, semiconducting solid-state devices, such as resonant tunneling diodes (RTDs)[5] and quantum cascade lasers (QCLs),[6,7] have also been developed simultaneously. RTDs have the advantage of operating at room temperature with sub-milliwatt-level output power up to a frequency of approximately 1 THz.[8,9] Recently, a 6×6 array of RTDs that operates at 0.45 THz with a maximum radiation power of 11.8 mW was reported.[10] Although low-temperature operation below 30 K is required to generate frequencies of 1 THz, QCLs can generate frequencies ranging from 1.2 to 5.4 THz with milliwatt-level power.[6,7] However, THz-QCLs using different frequency generation techniques operating at room temperature have recently been developed.[11]

In the last decade, THz wave emitters based on the AC Josephson effect[12] have been developed using a single crystal of the high-T_c superconductor $Bi_2Sr_2CaCu_2O_{8+\delta}$ (Bi2212). Single crystals of Bi2212 consist of insulating Bi_2O_2 layers and superconducting CuO_2 layers stacked alternately along the crystallographic c axis and are known as intrinsic Josephson junctions (IJJs).[13–15] Waves with frequencies in the terahertz range can be obtained by processing single crystals of Bi2212 into mesa structures and applying DC bias voltages across the IJJs.[16] According to previous studies, emission frequencies in the 0.15–2.4 THz range can be generated in free space by changing the size and shape of Bi2212 mesa structures.[16–21] Josephson emissions with a frequency range of 1–11 THz have been reported for small Bi2212 mesa structures.[22] The maximum power from a single-mesa device is approximately 30–100 μW.[17,20,23–26] An output power of approximately 0.6 mW can also be achieved from an array of three mesa structures.[26] More detailed characteristics of Bi2212-THz-wave emitters have been reviewed in several studies.[27–31]

We are interested in developing the IJJ device characteristics from the perspective of their crystal properties. Bi2212 single crystals are nonstoichiometric compounds, expressed as $Bi_{2+x}Sr_{2-x}CaCu_2O_{8+\delta}$. The nonstoichiometry of Bi/Sr, represented by x, significantly affects the superconducting characteristics of the compound; a smaller x results in a higher superconducting transition temperature.[32–34] In addition, the superconducting transition temperatures and the conductivities of the compound significantly depend on the amount of oxygen, thus depending on δ.[35] Based on these studies,[32–35] the IJJ device characteristics are likely to be controlled by varying the values of x and δ because the electrical properties of the IJJ device significantly depend on crystal conditions, such as carrier concentration and crystal defects. Clarifying the effects of x and δ on the device characteristics will help improve the performance of IJJ devices.

Although some studies have investigated the characteristics of IJJ emitters using crystals prepared under different annealing conditions[36] and Pb substitution,[37] to the best of our knowledge, the effects of the nonstoichiometry of Bi/Sr on the device characteristics have not been studied previously. In this study, Bi2212 single crystals with different x and δ values were prepared, and the variations in the crystal properties and device characteristics with these values were studied as a first step toward understanding the tendencies of the device characteristics associated with the crystal characteristics depending on the values of x and δ. The crystal and device characteristics of Bi2212 single crystals grown at $x = 0.05$, $x = 0.15$, and $x = 0.25$ as nominal compositions were evaluated. These x values were chosen because it is empirically known that larger single crystals can be grown in slightly Bi-rich phases. In addition, from the perspective of crystal characteristics, previous studies[32–34] have reported a reduction in the maximum superconducting transition temperature up to $x = 0.3$. Therefore, clear differences in the crystal properties and device characteristics were expected by comparing the samples with $x = 0.05$ and $x = 0.25$. Furthermore, the grown crystals were annealed under O_2 or N_2 gas flow conditions to change the amount of δ in each crystal and gain a broader understanding of the effect of annealing on the IJJ devices.

In this study, we first explain the compositional characteristics of crystals grown with different x values. Second, we compare the superconducting transition temperatures and unit cell parameters of the samples. Third, the characteristics of IJJ devices fabricated using the grown crystals are discussed. The experimental results reveal that the superconducting transition temperature and unit cell parameters highly depend on parameters, such as the Bi/Sr ratio and annealing conditions. The crystal characteristics, which depend on the parameter set, are reflected in the electrical characteristics of the Bi2212 THz-wave emitters. The data obtained from these studies can serve as a useful guide for the preparation of the crystals required for constructing IJJ THz-wave devices.

II. SAMPLE PREPARATIONS AND EXPERIMENTAL METHODS

$Bi_{2+x}Sr_{2-x}CaCu_2O_{8+\delta}$ single crystals prepared with nominal composition ratios of $x = 0.05$ (Bi/Sr = 2.05/1.95), $x = 0.15$ (2.15/1.85), and $x = 0.25$ (2.25/1.75) were grown using a floating zone furnace as described in previous studies.[38,39] To evaluate the sample characteristics and fabricate crystal chips for Bi2212 THz wave emitters, the grown crystals were cut into square shapes in the square-millimeter scale. Then, to adjust the oxygen content δ of the crystals, they were annealed for 4–6 days, either under O_2 gas flow at 400°C and a flow rate of 0.10 l/min or under N_2 gas flow at 600°C and a flow rate of 1.0 l/min. At the end of the annealing process, the crystals were quenched to fix their oxygen content.

In Sec. III, samples prepared using O_2- or N_2-annealed crystals with Bi/Sr ratios of 2.05/1.95 are referred to as Bi2.05-O_2 and Bi2.05-N_2, respectively. Similarly, the samples fabricated using the O_2- or N_2-annealed crystals with Bi/Sr ratios of 2.15/1.85 or 2.25/1.75 are referred to as Bi2.15–O_2, Bi2.15–N_2, Bi2.25–O_2, and Bi2.25–N_2, respectively.

To evaluate the chemical compositions of the grown crystals, a scanning electron microscope (SEM, TM3000, Hitachi) equipped with an energy dispersive spectroscopy (EDS) system was used. For EDS measurements, Bi2212 crystal chips fabricated using wet etching were used. The superconducting transition temperatures, T_cs, of the crystals were determined from the temperature dependences of their magnetic susceptibilities using a SQUID magnetometer (MPMS, Quantum Design). For the magnetic susceptibility measurements, single crystals with a size of 2 mm^2 were used, and a magnetic field of 2 Oe was applied parallel to the c axis of the sample.

Wet etching was used to fabricate the Bi2212 crystal chip, which was established by our group[40,41] based on previous

08 October 2024 06:40:49

© Author(s) 2024

studies.[42–45] Briefly, the crystals were initially cleaved on both sides to prepare thin single-crystal plates with thicknesses of 3–5 μm. Subsequently, silver and gold were deposited on both sides of the crystal. The total thickness of the metal films was in the range of 20–50 nm. The crystal was then glued onto a sapphire plate, and photolithography techniques were used to create photoresist mask patterns on the crystal surface. The crystals were processed into rectangular chips using a wet-etching method. Subsequently, these chips were assembled as Bi2212 THz wave emitters using a sandwich structure developed by our group.[20]

In the sandwich structure, a crystal chip is simply sandwiched by two sapphire plates on which metallic electrodes are patterned. These parts are held by metallic rigs and fixed with screws. The Joule heat generated at the crystal chip can be removed using these structures. The interface between the crystal chips and the sapphire substrate is important for thermal management, as well as for electrical contact between the chip and electrodes. By properly configuring them, for example, a dc bias voltage with 2.2 mV/junction can be applied to a crystal chip with dimensions of 58–66 $\times$ 350 $\times$ 4.7 μm^3 at 15 K.[20] Recently, thicker mesa structures for high power emission have been developed considering a good heat-removal interface structure, and 0.7 mV/junction at 4.2 K was obtained from a cylindrical mesa with 400 $\times$ 13 μm^2.[45] The continuous development of thermal management is an important subject to improve the emission intensity and frequency.

To characterize the fabricated crystal chips, x-ray diffraction was performed with an ω–2θ scan to measure the distribution of the unit cell parameters along the c axis of the samples. A four-circle diffractometer was used at BL-4C, the Photon Factory of the High Energy Accelerator Research Organization (KEK). The beam shape at the sample position was elliptical, with 0.6 mm vertically and 0.8 mm horizontally. The incident x-ray energy was set to be 8.8 keV using a Si(111) double-crystal monochromator. Under the present measurement conditions, a precise distribution of the unit cell parameters on the order of 10^{-2} Å can be obtained.

To characterize the Bi2212 THz emitter, it was mounted on the cold finger of a helium-flow type of cryostat (Oxford Instruments, CF1104) equipped with optical windows. An FeRh thermometer was placed on the cold finger. The measured temperature T_b directly indicates the temperature of the cold finger and not that of the crystal chip itself. Electrical characteristics of the devices were measured using a conventional two-terminal method. An InSb hot-electron bolometer (HEB) (QMC Instruments, QFI/2BI) was used to detect electromagnetic waves emitted from the devices.[46]

It is sometimes difficult to use the same piece of crystal for the above measurements, primarily because of the technical limitations of sample preparation. For example, to fabricate crystal chips using a crystal that was evaluated by a magnetic susceptibility measurement, there are sometimes sample losses in the fabrication processes, such as failure of crystal cleaving and over-etching of the samples. Therefore, different crystal pieces were used to evaluate the samples. The single crystals used for the THz wave emitters and magnetic susceptibility measurements were different; however, they were obtained from the same site on the grown crystal rod and were annealed simultaneously. The crystal chips used for x-ray diffraction and device characteristic measurements were different but were fabricated simultaneously from the same single-crystal fragment.

III. RESULTS AND DISCUSSION

Herein, the results related to the crystal characteristics depending on x and δ are presented. First, we explain the compositional characteristics of the crystals grown with different x values. Next, we compare the superconducting transition temperatures and unit cell parameters of the samples. The crystal characteristics evaluated in this study exhibit some differences depending on the sample. The main purpose of this evaluation is to determine the trends in the crystal conditions as x and δ varied.

Table I lists the chemical compositions of the fabricated crystal chips as determined by the EDS analysis. The typical chip dimensions were ≈80 $\times$ 200–400 $\times$ 2–6 μm^3. The values evaluated in Table I were normalized such that the sum of Bi, Sr, and Ca was five. For normalization, Cu was not included because the observed EDS data for Cu had a larger standard deviation than those for the other elements. Unfortunately, the reason for the large standard deviation is unknown. To estimate the precise chemical composition, a quantitative analysis, such as that performed on an electron probe microanalyzer (EPMA), is required.

The results showed that the Bi/Sr ratios of the grown crystals were higher than those of the nominal compositions and increased with increasing Bi/Sr ratios of the nominal compositions. The grown crystals tended to prefer Bi-rich phase conditions, as reported in previous studies.[32,33] The samples with $x = 0.05$ showed a decrease in the amount of Ca. This feature may be reflected in the T_c characteristics, which will be discussed later.

Figure 1 shows the temperature dependence of the normalized magnetic susceptibility of bulk crystals. The onsets of the superconducting transition temperatures T_c of the crystals estimated from the measurements are summarized in Table II.

The O_2-annealed crystals with different Bi/Sr ratios show similar T_c values, whereas the T_c values of the N_2-annealed crystals significantly depend on the Bi/Sr ratios, even under the same annealing conditions. According to a previous study,[34] the T_c values of samples with higher x values were strongly suppressed for small values of δ. The observed trend was consistent with that reported in the previous study. The difference in T_c between the samples with $x = 0.05$ and $x = 0.15$ may be reflected in the difference in the amount of Ca. If the Ca^{2+} sites are substituted with

TABLE I. EDS analysis data of fabricated Bi2212 crystal chips. Numbers in parentheses are standard deviations of the last significant digit.

Sample	Nominal Bi/Sr ratio	Bi	Sr	Ca	Evaluated Bi/Sr ratio
Bi2.05–N_2	1.051	2.24(3)	1.85(3)	0.91(4)	1.21
–O_2		2.24(3)	1.87(3)	0.89(2)	1.20
Bi2.15–N_2	1.162	2.23(2)	1.76(2)	1.02(2)	1.27
–O_2		2.21(4)	1.80(4)	0.98(4)	1.23
Bi2.25–N_2	1.286	2.27(2)	1.70(1)	1.02(2)	1.33
–O_2		2.27(2)	1.69(2)	1.05(2)	1.34

08 October 2024 06:40:49

© Author(s) 2024

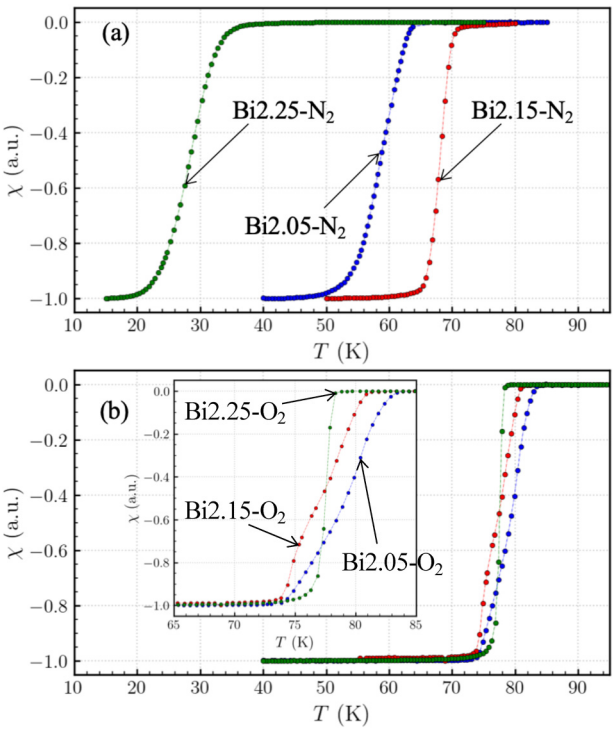

FIG. 1. Temperature dependence of normalized magnetic susceptibilities of the grown crystals with different Bi/Sr ratios: (a) annealed under N_2 gas flow at 600°C and (b) annealed under O_2 gas flow at 400°C. The inset of Fig. 1(b) displays the magnification plot of the O_2 annealed samples around T_c. The observed susceptibility data were normalized to be −1 using the values obtained at the lowest measurement temperatures. The results for the zero-field cooling data are plotted.

Bi^{3+}, the valence difference between these ions reduces the hole density in the CuO_2 plane.[33,48] This is related to the decrease in the T_c value of the sample with $x = 0.05$. We will discuss the tendency of the valence difference in the sample later.

The information of T_c of as-grown crystals and typical annealing conditions of the optimal doping for the samples would be helpful for understanding the characteristics of prepared crystals as well as for preparing the crystals for the emitters. Table II lists the T_c values of the as-grown crystals for $x = 0.05$, $x = 0.15$, and $x = 0.25$. Based on previous studies[32,35] and our experimental experience, the expected annealing conditions of optimal doping for $x = 0.05$, $x = 0.15$, and $x = 0.25$ are ≈0.1%-O_2 at ≈700°C, ≈0.1%-O_2 at ≈500°C, and 100%-O_2 with a flow rate of 0.10 L/min at ≈600°C, respectively. To prepare the gas condition of ≈0.1%-O_2, a mixture of two gases, N_2 with a flow rate of 0.60 l/min and O_2 with a flow rate of 0.20 ml/min, were used, and these flow rates were then adjusted to ≈0.1%-O_2 by monitoring an oxygen sensor installed downstream of the gas flow path. These conditions depend on the size of the crystals and atmospheric gases owing to the degassing of oxygen from the samples.

TABLE II. T_c-onsets of the prepared crystals.

Bi/Sr ratio	N_2 annealed (K)	O_2 annealed (K)	As-grown (K)
2.05/1.95	63.0	82.7	89.1
2.15/1.85	70.0	81.0	84.0
2.25/1.75	37.0	78.2	72.0

Figures 2(a)–2(c) show the ω–2θ scans measured around 00$\underline{26}$ for the crystal chips with different x values. Data were normalized to the maximum peak intensities of the scans. The N_2-annealed samples exhibited almost a single peak in the ω–2θ scan. With increasing Bi/Sr ratio, the peak position shifted to a higher angle from $2\theta = 72.64°$ to 72.82°, indicating a reduction in the unit cell

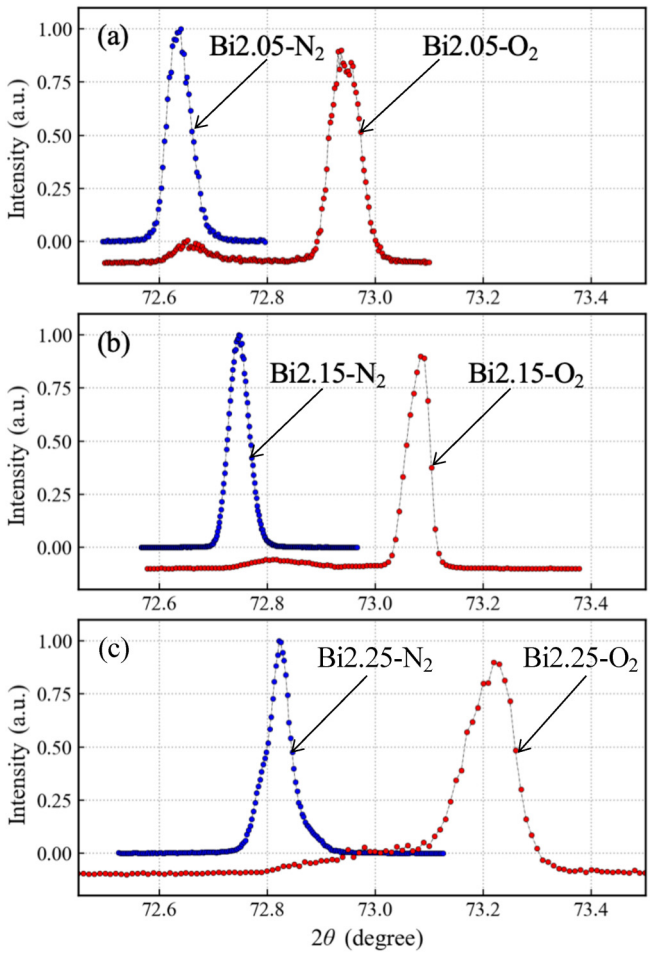

FIG. 2. Normalized data plot of the ω–2θ scan measured around 00$\underline{26}$ for the (a) $x = 0.05$, (b) $x = 0.15$, and (c) $x = 0.25$ samples. The data for the N_2 and O_2 annealed samples are displayed in blue and red colored symbols, respectively. The data plots for O_2 annealed samples are shifted vertically to avoid overlapping those for the N_2 annealed ones.

08 October 2024 06:40:49

© Author(s) 2024

parameter c. In general, the curve profile shows the distribution of unit cell parameters and strain in the samples. The curve profiles of each N_2-annealed sample show that these distributions are almost comparable, although the curve profile of Bi2.25–N_2 exhibited a shoulder on the lower-angle side.

The O_2-annealed samples differ from the N_2-annealed samples and show two distinct peaks. The weak signal observed on the lower side of 2θ originates from the contribution of the surface of the crystals. The oxygen content on the crystal surface of the O_2-annealed sample was easily reduced during metal evaporation, forming electrodes on the crystal surface. This is related to the stability of the oxygen in the compound, as discussed in our previous study.[47]

The stronger peak observed at a higher 2θ shifted to a higher angle from $2\theta = 72.94°$ to $73.22°$ with increasing Bi/Sr ratio. The weak signal also shifted to a higher angle from $2\theta = 72.66°$ to $73.00°$. The linewidth of each O_2-annealed sample was broader than that of the N_2-annealed sample. For the Bi2.25–O_2 sample, a clear broadening of the linewidth was observed, indicating a lower homogeneity of the unit cell parameter c.

A shift in the peak position of the ω–2θ scan to a higher angle indicates a decrease in the unit cell parameter c. Figure 2 shows that the unit cell parameter c decreased not only for the O_2-annealed samples, but also when the Bi/Sr ratio was increased. These tendencies are consistent with those observed in previous studies[34,48,49] and are discussed later. The unit cell parameters c estimated from the ω–2θ scans are summarized in Table III.

Figure 3 shows a comparison of the device characteristics fabricated using N_2-annealed crystals. The dimensions of the fabricated crystal chips for the THz wave emitters are $78 \times 174 \times 4.0\,\mu m^3$ for Bi2.05-N_2, $55\,\mu m \times 181\,\mu m \times 2.9\,\mu m$ for Bi2.15–N_2 and $52 \times 385 \times 2.5\,\mu m^3$ for Bi2.25–N_2, respectively. For the device characteristics, we focused on the results of the N_2-annealed samples to obtain a meaningful comparison of their crystal characteristics. In our previous study, the device characteristics of the O_2-annealed sample were complicated because of the higher carrier concentration and inhomogeneity of the oxygen content of the surface part of the crystal chips.[47] For the samples with $x = 0.05$ and 0.15, we also confirmed that the O_2-annealed samples prepared in this study show similar tendencies to those obtained in a previous study.[47]

In addition, we only discuss whether these devices exhibit electromagnetic wave emission and compare the device characteristics by using the above crystal chips, which we have fabricated so far. Particularly, to obtain further understanding of the device characteristics based on the cavity resonance condition depending on the chip size, a comparison of chips with similar dimensions is required. Therefore, to precisely understand the differences in the radiation characteristics of the samples, we plan to perform further experiments using crystal chips with similar dimensions and an increased number of sample measurements.

TABLE III. Estimated unit cell parameter c for the prepared crystal chips.

Bi/Sr ratio	N_2 annealed (Å)	O_2 annealed (Å)
2.05/1.95	30.91	30.82
2.15/1.85	30.88	30.75
2.25/1.75	30.86	30.69

The insets of Fig. 3 show the temperature dependence of the c axis resistance (RT) of the Bi2212 crystal chips assembled in a sandwich structure. In all cases, the c axis resistance increased as the temperature decreased from room temperature to lower temperatures but decreased significantly around T_c. T_c of Bi2.25–N_2 was lower than that of Bi2.05–N_2 and Bi2.15–N_2. This trend of T_c is consistent with the temperature dependence of the magnetic susceptibility (MT) data, as shown in Fig. 1(a). The differences in the values of T_c between the RT and MT data likely originated from the differences in the crystal batches used for each measurement. However, a precise discussion of the sample conditions based on the RT data is difficult because the data include extrinsic resistance, other than the resistance of the electrode of a metallic thin film prepared on a sapphire plate;[20] for example, the effects of the surface conditions of the crystal chips prepared after wet etching and the contact between the chips and electrodes may be included in the resistance.

Figures 3(a-1), 3(b-1), and 3(c-1) show the current–voltage characteristics (IVCs) of Bi2.05-N_2, Bi2.15–N_2, and Bi2.25–N_2 measured at various bath temperatures T_B. In the IVCs, the voltage generated as the applied current increased was low but suddenly increased to a large voltage value when the current exceeded the critical current I_c. When the current decreased, the voltage state persisted up to a certain current value, and a hysteresis loop was observed in the IVCs. The size of the hysteresis loop varied with T_B and decreased with increasing T_B. The critical current I_c varied with the Bi/Sr ratio and decreased with an increasing ratio, as shown in Fig. 3. To evaluate the difference in the I_c values, the critical current density values J_c at low T_B values were estimated from the I_c values and the areas of the crystal chips. The estimated values of J_c for Bi2.05–N_2, Bi2.15–N_2, and Bi2.25–N_2 were ≈140, ≈160, and ≈15 A/cm^2, respectively. The J_c values of the Bi2.05-N_2 and Bi2.15–N_2 samples were comparable to those reported in previous studies;[36] however, the J_c value of the Bi2.25–N_2 sample was strongly suppressed. This is a characteristic feature of the substitution effect on the device characteristics.

In Figs. 3(a-2), 3(b-2), and 3(c-2), the radiation intensity detected by the HEB, denoted V_{bol}, is plotted as a function of the bias voltage applied to the crystal chip. Data were acquired simultaneously during IVC measurements. As shown in Figs. 3(a-2) and 3(b-2), the devices made of Bi2.05-N_2 and Bi2.15–N_2 show the emission of electromagnetic waves at the return branches of the IVCs. According to the previous studies,[20,24] the detected emission power P can be estimated by $P = 2\sqrt{2}\,V_{bol}/\alpha$, where $\alpha = 3.3$ mV/nW is the system optical responsivity calibrated with blackbody radiation. Therefore, the observed V_{bol} of ≈10 mV for Bi2.05–N_2 and Bi2.15–N_2 correspond to $P \approx 9$ nW.

Conversely, no electromagnetic-wave emission was observed for Bi2.25–N_2. The maximum applied bias voltage on the hysteresis loop of Bi2.25–N_2 was smaller than that of the other two devices. In this case, it was difficult to generate high-frequency current based on the AC Josephson effect. The generated current did not match the cavity resonance frequencies determined by the shapes

08 October 2024 06:40:49

© Author(s) 2024

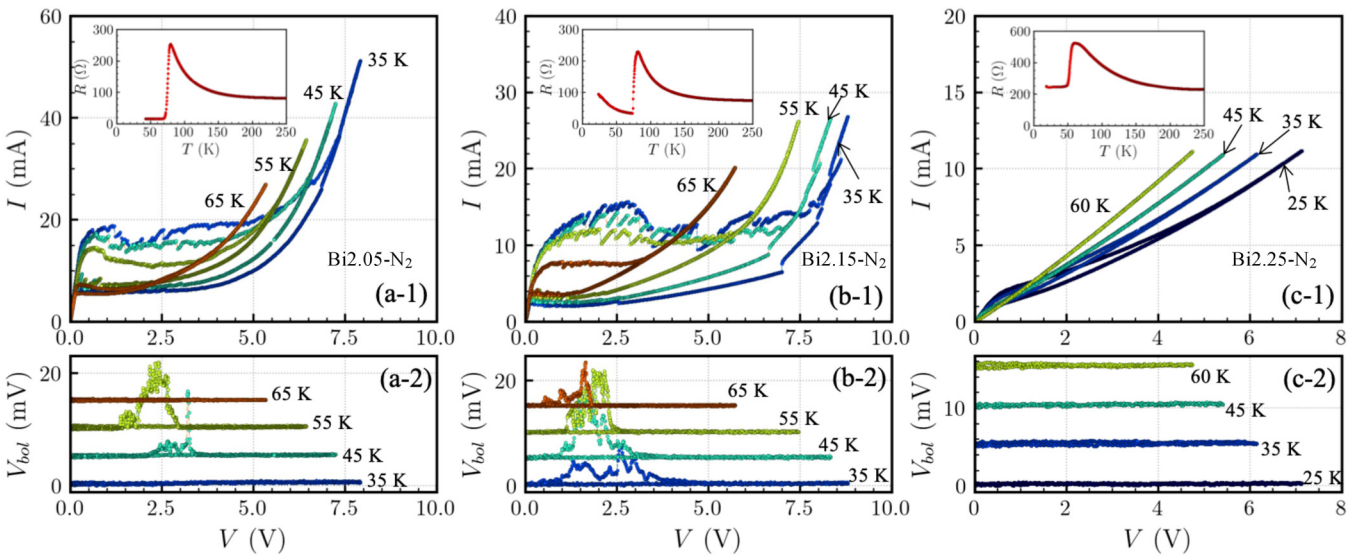

FIG. 3. Typical temperature dependence of the IVCs for Bi2.05-N_2 (a-1), Bi2.15–N_2 (b-1), and Bi2.25–N_2 (c-1). The radiation intensities detected by the HEB, V_{bol}, are plotted as a function of the applied bias voltages for Bi2.05-N_2 (a-2), Bi2.15–N_2 (b-2), and Bi2.25–N_2 (c-2). The temperature shown with the curve indicates T_b of the sample. The insets in the IVC-plots show the temperature dependence of the *c* axis resistance.

and dimensions of the crystal chips. This was most likely the reason for the lack of emissions in the Bi2.25–N_2 sample.

In the final part of this paper, for basic understanding of the experimental results, we discuss the variation in the device characteristics owing to the Bi/Sr substitution and annealing effects, although these two effects are connected to each other.[48,49] In addition, we consider a simple case in which the influence of the substitution or introduction of Bi, Sr, and O atoms in Bi2212 crystals is observed mainly along the crystallographic *c* axis.

To understand the effect of Bi/Sr substitution, information on the valency and ionic radii of Bi and Sr in Bi2212 crystals is helpful. The valency of the elements in the compound is Bi^{3+} and Sr^{2+}. The ionic radii of Bi^{3+} (eight coordinates) and Sr^{2+} (nine coordinates) are 1.17 and 1.31 Å.[50] In addition, according to previous studies,[32,33,48] this compound has a tendency for the Sr^{2+} sites located next to the apical oxygen to be easily substituted with Bi^{3+} because of the greater stability of the crystal structure.

Based on the above information, an increase in the ratio of Bi^{3+} substitutions at the Sr^{2+} sites in the compound is expected to reduce the unit cell parameter *c* because of the substitution of the small ionic radius of Bi^{3+}. In addition, owing to the valence difference between Bi^{3+} and Sr^{2+}, the hole content in the CuO_2 plane decreases. This behavior can also be understood from the substitution effect of the Ca^{2+} site by Bi^{3+} and Y^{3+}.[32,33,48] Moreover, an excessive increase in the Bi content caused inhomogeneity in the crystal structure and crystal defects, such as stacking faults in the compound. These effects would appear in transport characteristics.

The dependence of the experimental results on the Bi/Sr ratio can be understood from these perspectives. As shown in Fig. 2, the samples with higher *x* values exhibited a smaller unit cell parameter *c*. The strong suppression of the T_c value of Bi2.25–N_2 is mainly from the reduction in the hole content of the CuO_2 plane due to the substitution of Sr^{2+} sites by Bi^{3+}. The device characteristics are shown in Fig. 3. The lower hole content characteristics of the Bi2.25–N_2 sample were reflected in the lowest J_c and T_c values. Based on the results for the unit cell parameter *c*, the J_c value of Bi2.25–N_2 is expected to be larger than those of the other samples because Bi2.25–N_2 is expected to have the shortest IJJ tunneling barrier. However, the experimental results indicate that the dominant effect on the J_c value of the sample was the hole content of the CuO_2 plane.

Next, we discuss the effect of oxygen content in the crystal. The oxygen content can be tuned by varying the annealing conditions, such as atmospheric gas and heating temperatures.[35] According to previous studies,[32,33,48] excess oxygen atoms are located in or near the Bi_2O_2 insulating layers. In addition, an increase in the oxygen content is reflected as a reduction in the distance between the BiO double layers and an increase in the hole content of the CuO_2 layers owing to the electric charge balance.

As shown in Figs. 1 and 2, as the oxygen content increases, the transition temperature T_c increases, and the unit cell parameter *c* decreases. This feature is reflected in the device characteristics as an increase in the maximum critical current I_c owing to the increase in the carrier concentration of the sample as well as the reduction in the distance between the BiO double layers. The device characteristics of the oxygen-annealed samples are not presented here. The characteristics mentioned above can be found not only in our previous paper[47] but also in a previous study in which slightly underdoped crystals were used.[36]

The data shown in Fig. 2 are beneficial for the preparation of crystal chips. The data indicate that the oxygen-annealed samples had an inhomogeneous oxygen content. This factor has an effect

08 October 2024 06:40:49

© Author(s) 2024

on various device characteristics. Therefore, during the fabrication processes of crystal chips, care must be taken to maintain the homogeneity of the oxygen content in the crystals.

Finally, based on previous discussion and the Josephson relation, we discuss how the characteristics of the material are reflected in the device characteristic. According to the Josephson relation for a conventional superconducting Josephson junction, the current density J_{ac} in the resistive state is $J_{ac} = J_c \sin[(2eV/\hbar)\ t + \text{const.}]$, where e is the electric charge, $\hbar$ is Planck's constant divided by 2π, t is the time, and V is the bias voltage applied to the junction. Typically, J_c is proportional to junction tunnel conductance.[51] Hence, in the case of IJJs, J_c is characterized by material characteristics, such as the unit cell parameter c, carrier density, and Bi/Sr nonstoichiometry.

The experimental results discussed here show that the value of J_c can be tuned by controlling the Bi/Sr ratios and the oxygen contents of the compound. The primary effect of the change in these values on the IJJs is the adjustment of the carrier content of the sample. To increase the emission power of terahertz waves from the devices, a higher value of J_c would be better according to the Josephson relation. This feature can be clearly seen in the results for the Bi2.25–N_2 sample, which shows no emission owing to the strong suppression of the IVCs related to lower J_c and T_c. For the suppression of emission, the inhomogeneity of the crystal will also be reflected, although further studies are needed to clarify its effect on IJJ devices. As discussed in a previous study,[32] the decrease in the value of the maximum T_c with increasing x value originates from the inhomogeneity of the crystal structure due to Bi/Sr nonstoichiometry.

The high J_c sample prepared by increasing the oxygen contents is unsuitable for the current device structure because of the requirement of the application of a large amount of bias current to obtain a resistive state of IJJs, the requirement of good heat-removal structures owing to the higher current application, and the inhomogeneity of the oxygen content of the crystal surface. Consequently, it is expected that a crystal prepared with a lower x value and slightly under-doped conditions would be better for the device to operate at a higher temperature with higher emission power.

In summary, we demonstrated that the crystal properties of Bi2212 affect the characteristics of THz-wave-emitting devices made from Bi2212. The results of this study indicate that the carrier concentration in a crystal chip can be adjusted by controlling the Bi/Sr ratio and δ. In addition, the results suggest that the preparation of crystals, including annealing under appropriate conditions depending on the Bi/Sr ratio, is crucial for producing the desired IJJ devices. Although further evaluation of the device characteristics with a similar number of carriers for each Bi/Sr ratio is required to fully understand the effect of Bi/Sr substitution on IJJ devices, the experimental results presented herein provide a helpful guide for preparing crystals for THz-wave-emitting devices.

IV. CONCLUSION

Bi2212 crystals with different Bi/Sr ratios and δ values were prepared, and the crystal and device characteristics were compared as a first step toward understanding the device characteristics related to the crystal characteristics. No significant difference was observed in the electric device characteristics between samples with Bi/Sr = 2.05/1.95 and 2.15/1.85. However, for the sample with Bi/Sr = 2.25/1.75, a significant change in device properties was observed. This feature can be understood primarily from the change in the number of carriers in the crystals, which can be adjusted by controlling the Bi/Sr ratio and δ. These results indicate that the preparation of crystals, including annealing under appropriate conditions depending on the Bi/Sr ratio, is crucial for producing desired IJJ devices. The experimental results presented herein provide a helpful guide for preparing crystals for THz-wave-emitting devices.

ACKNOWLEDGMENTS

This study was supported by the Japan Society for the Promotion of Science Grant-in-Aid for Scientific Research (C) No. JP17K05018 and Research (B) Nos. JP20H02590, JP21H01377, and JP23H01819. This study was also supported by TIA-Kakehashi grants (Nos. 2018-43 and 2019-47). The x-ray diffraction measurements were performed with the approval of the Photon Factory Program Advisory Committee (Proposal No. 2019G634).

AUTHOR DECLARATIONS

Conflict of Interest

The authors have no conflicts to disclose.

Author Contributions

M. Nakayama: Conceptualization (supporting); Investigation (equal); Resources (equal); Visualization (lead); Writing – original draft (lead); Writing – review & editing (equal). **S. Nakagawa:** Conceptualization (equal); Investigation (equal); Resources (equal); Writing – review & editing (supporting). **T. Yamaguchi:** Investigation (equal). **H. Minami:** Conceptualization (supporting); Project administration (equal); Resources (equal); Supervision (supporting); Writing – review & editing (equal). **K. Kadowaki:** Resources (equal); Supervision (supporting). **H. Nakao:** Conceptualization (supporting); Investigation (supporting); Project administration (supporting); Resources (equal); Supervision (supporting); Writing – review & editing (supporting). **T. Mochiku:** Conceptualization (supporting); Project administration (supporting); Supervision (supporting); Writing – review & editing (supporting). **M. Tsujimoto:** Project administration (supporting); Resources (supporting); Supervision (supporting); Writing – review & editing (supporting). **S. Ishida:** Conceptualization (supporting); Project administration (supporting); Resources (supporting); Supervision (equal); Writing – review & editing (supporting). **H. Eisaki:** Conceptualization (supporting); Project administration (supporting); Resources (equal); Supervision (equal); Writing – review & editing (supporting). **T. Kashiwagi:** Conceptualization (equal); Funding acquisition (lead); Investigation (equal); Project administration (equal); Resources (equal); Supervision (equal); Writing – original draft (lead); Writing – review & editing (lead).

DATA AVAILABILITY

The data that support the findings of this study are available within the article.

08 October 2024 06:40:49

© Author(s) 2024

REFERENCES

[1]B. Ferguson and X. C. Zhang, Nat. Mater. **1**, 26 (2002).
[2]M. Tonouchi, Nat. Photonics **1**, 97 (2007).
[3]S. S. Dhillon, M. S. Vitiello, E. H. Linfield, A. G. Davies, M. C. Hoffmann, J. Booske, C. Paoloni, M. Gensch, P. Weightman, G. P. Williams *et al.*, J. Phys. D: Appl. Phys. **50**, 043001 (2017).
[4]K. Okada, K. Serita, Q. Cassar, H. Murakami, G. MacGrogan, J. Guillet, P. Mounaix, and M. Tonouchi, J. Phys.: Photon. **2**, 044008 (2020).
[5]S. Suzuki, M. Asada, A. Teranishi, H. Sugiyama, and H. Yokoyama, Appl. Phys. Lett. **97**, 242102 (2010).
[6]B. S. Williams, Nat. Photon. **1**, 517 (2007).
[7]C. Walther, M. Fischer, G. Scalari, R. Terazzi, N. Hoyler, and J. Faist, Appl. Phys. Lett. **91**, 131122 (2007).
[8]S. Suzuki, M. Shiraishi, H. Shibayama, and M. Asada, IEEE J. Sel. Top. Quantum Electron. **19**, 8500108 (2013).
[9]K. Kasagi, S. Suzuki, and M. Asada, J. Appl. Phys. **125**, 151601 (2020).
[10]Y. Koyama, Y. Kitazawa, K. Yukimasa, T. Uchida, T. Yoshioka, K. Fujimoto, T. Sato, J. Iba, K. Sakurai, and T. Ichikawa, IEEE Trans. Terahertz Sci. Technol. **5**, 510 (2022).
[11]K. Fujita, S. Jung, Y. Jiang, J. H. Kim, A. Nakanishi, A. Ito, M. Hitaka, T. Edamura, and M. A. Belkin, Nanophotonics **7**, 1795 (2018).
[12]B. D. Josephson, Phys. Lett. **1**, 251 (1962).
[13]R. Kleiner, F. Steinmeyer, G. Kunkel, and P. Müller, Phys. Rev. Lett. **68**, 2394 (1992).
[14]R. Kleiner and P. Müller, Phys. Rev. B **49**, 1327 (1994).
[15]A. A. Yurgens, Supercond. Sci. Technol. **13**, R85 (2000).
[16]L. Ozyuzer, A. E. Koshelev, C. Kurter, N. Gopalsami, Q. Li, M. Tachiki, K. Kadowaki, T. Yamamoto, H. Minami, H. Yamaguchi *et al.*, Science **318**, 1291 (2007).
[17]T. Kitamura, T. Kashiwagi, T. Yamamoto, M. Tsujimoto, C. Watanabe, K. Ishida, S. Sekimoto, K. Asanuma, T. Yasui, K. Nakade *et al.*, Appl. Phys. Lett. **105**, 202603 (2014).
[18]M. Ji, J. Yuan, B. Gross, F. Rudau, D. Y. An, M. Y. Li, X. J. Zhou, Y. Huang, H. C. Sun, Q. Zhu *et al.*, Appl. Phys. Lett. **105**, 122602 (2014).
[19]T. Kashiwagi, K. Sakamoto, H. Kubo, Y. Shibano, T. Enomoto, T. Kitamura, K. Asanuma, T. Yasui, C. Watanabe, K. Nakade *et al.*, Appl. Phys. Lett. **107**, 082601 (2015).
[20]T. Kashiwagi, T. Yamamoto, H. Minami, M. Tsujimoto, R. Yoshizaki, K. Delfanazari, T. Kitamura, C. Watanabe, K. Nakade, T. Yasui *et al.*, Phys. Rev. Appl. **4**, 054018 (2015).
[21]H. Sun, S. Chen, Y. L. Wang, G. Sun, J. Chen, T. Hatano, V. P. Koshelets, D. Koelle, R. Kleiner, H. Wang, and P. Wu, Appl. Sci. **13**, 3469 (2023).
[22]E. A. Borodiansky and V. M. Krasnov, Nat. Commun. **8**, 1742 (2017).
[23]D. Y. An, J. Yuan, N. Kinev, M. Y. Li, Y. Huang, M. Ji, H. Zhang, Z. L. Sun, L. Kang, B. B. Jin *et al.*, Appl. Phys. Lett. **102**, 092601 (2013).
[24]S. Sekimoto, C. Watanabe, H. Minami, T. Yamamoto, T. Kashiwagi, R. A. Klemm, and K. Kadowaki, Appl. Phys. Lett. **103**, 182601 (2013).
[25]K. Kadowaki, M. Tsujimoto, K. Delfanazari, T. Kitamura, M. Sawamura, H. Asai, T. Yamamoto, K. Ishida, C. Watanabe, S. Sekimoto *et al.*, Physica C **491**, 2 (2013).
[26]T. M. Benseman, K. E. Gray, A. E. Koshelev, W.-K. Kwok, U. Welp, H. Minami, K. Kadowaki, and T. Yamamoto, Appl. Phys. Lett. **103**, 022602 (2013).
[27]U. Welp, K. Kadowaki, and R. Kleiner, Nat. Photon. **7**, 702 (2013).
[28]I. Kakeya and H. Wang, Supercond. Sci. Technol. **29**, 073001 (2016).
[29]T. Kashiwagi, H. Kubo, K. Sakamoto, T. Yuasa, Y. Tanabe, C. Watanabe, T. Tanaka, Y. Komori, R. Ota, G. Kuwano *et al.*, Supercond. Sci. Technol. **30**, 074008 (2017).
[30]R. Kleiner and H. Wang, J. Appl. Phys. **126**, 171101 (2019).
[31]K. Delfanazari, R. A. Klemm, H. J. Joyce, D. A. Ritchie, and K. Kadowaki, Proc. IEEE **108**, 721 (2020).
[32]H. Eisaki, N. Kaneko, D. L. Feng, A. Damascelli, P. K. Mang, K. M. Shen, Z.-X. Shen, and M. Greven, Phys. Rev. B **69**, 064512 (2004).
[33]H. Hobou, S. Ishida, K. Fujita, M. Ishikado, K. M. Kojima, H. Eisaki, and S. Uchida, Phys. Rev. B **79**, 064507 (2009).
[34]S. Yamashita, T. Kasai, T. Fujii, T. Watanabe, and A. Matsuda, Physica C **470**, S170–S172 (2010).
[35]T. Watanabe, T. Fujii, and A. Matsuda, Phys. Rev. Lett. **79**, 2113 (1997).
[36]L. Ozyuzer, Y. Simsek, H. Koseoglu, F. Turkoglu, C. Kurter, U. Welp, A. E. Koshelev, K. E. Gray, W. Kwok, T. Yamamoto, and K. Kadowaki, Supercond. Sci. Technol. **22**, 114009 (2009).
[37]M. Tsujimoto, Y. Maeda, H. Kambara, A. Elarabi, Y. Yoshioka, Y. Nakagawa, Y. Wen, T. Doi, H. Saito, and I. Kakeya, Supercond. Sci. Technol. **28**, 105015 (2015).
[38]T. Mochiku and K. Kadowaki, Physica C **235–240**, 523 (1994).
[39]T. Mochiku, K. Hirata, and K. Kadowaki, Physica C **282-287**, 475 (1997).
[40]Y. Shibano, T. Kashiwag, Y. Komori, K. Sakamoto, Y. Tanabe, T. Yamamoto, H. Minami, R. A. Klemm, and K. Kadowaki, AIP Adv. **9**, 015116 (2019).
[41]T. Imai, T. Kashiwagi, S. Nakagawa, M. Nakayama, J. Kim, G. Kuwano, M. Tsujimoto, H. Minami, and K. Kadowaki, Jpn. J. Appl. Phys. **60**, 126501 (2021).
[42]T. Kato, H. Ishida, H. Suematsu, K. Yasui, and K. Hamasaki, Cryogenics **52**, 398 (2012).
[43]T. Nishikata, T. Kato, Y. Kotaki, H. Suematsu, A. Kawakami, and K. Yasui, Jpn. J. Appl. Phys. **53**, 04EJ02 (2014).
[44]E. A. Vopilkin, A. V. Chiginev, L. S. Revin, A. N. Tropanova, I. Yu. Shuleshova, A. I. Okhapkin, A. D. Shovkun, A. B. Kulakov, and A. L. Pankratov, Supercond. Sci. Technol. **28**, 045006 (2015).
[45]L. S. Revin, E. A. Vopilkin, A. L. Pankratov, S. A. Kraev, A. A. Yablokov, and A. B. Kulakov, Supercond. Sci. Technol. **31**, 104001 (2018).
[46]T. Kashiwagi, M. Tsujimoto, T. Yamamoto, H. Minami, K. Yamaki, K. Delfanazari, K. Deguchi, N. Orita, and T. Koike *et al.*, Jpn. J. Appl. Phys. **51**, 010114 (2012).
[47]S. Nakagawa, T. Shizu, T. Imai, M. Nakayama, J. Kim, H. Minami, K. Kadowaki, M. Tsujimoto, H. Nakao, H. Eisaki, S. Ishida, T. Mochiku, Y. Hasegawa, and T. Kashiwagi, J. Appl. Phys. **133**, 163904 (2023).
[48]H. W. Zandbergen, W. A. Groen, A. Smit, and G. van Tendeloo, Physica C **168**, 426 (1990).
[49]W. A. Groen, D. M. de Leeuw, and L. F. Feiner, Physica C **165**, 55 (1990).
[50]R. D. Shannon, Acta Cryst. **A32**, 751 (1976).
[51]V. Ambegaokar and A. Baratoff, Phys. Rev. Lett. **11**, 104 (1963).

08 October 2024 06:40:49

© Author(s) 2024